Metall. Res. Technol. **119**, 314 (2022)

https://doi.org/10.1051/metal/2022029

&Metallurgical Research Technology

Available online at:
www.metallurgical-research.org

Regular Article

Effect of multi-angle parameter on fluid flow characteristics of swirl-type oxygen lance

Xi Wang, Peng Han*, and Kun Liu

School of Materials and Metallurgy, University of Science and Technology Liaoning, 114051 Anshan, China

Received: 2 December 2021 / Accepted: 29 March 2022

Abstract. The supersonic jet characteristics of the oxygen lance nozzle play an important role in converter melting. In this study, the jet characteristics of swirl-type oxygen lance were investigated by numerical simulation. The velocity field, jet coalescence behavior and jet impact cavity area of swirl-type oxygen lance with different inclination and swirl angles were analyzed. The results demonstrate that compared with the traditional oxygen lance, the swirl angle accelerates the attenuation of the jet. However, the tangential velocity of jet is conducive to the rapid melting of the slag in the steelmaking process. With the increase of swirl angle and inclination angle, the velocity of jet decreases, the temperature of jet increases and the independence between jets is improved. With the increase of the swirl angle, the tangential velocity of the swirl-type oxygen lance increases, but the possibility of slag adhering to the nozzle surface increases. The effective impact area varies non-monotonically with the swirl angle. The optimum inclination and swirl angle of the swirl-type oxygen lance for a 260 t converter are 15° and 10° respectively. When the oxygen flow rate increases, the decay of jet velocity decreases and the effective impact area increases.

Keywords: swirling jet / jet coalescence / impact area / oxygen lance

1 Introduction

In modern steelmaking, the behavior of oxygen jet has an important influence on the movement and mixing effect of molten steel in the converter. The supersonic oxygen jet at the slag-metal interface can cause liquid steel splashing and fluid movement in the molten pool, which forms kinetic conditions conducive to optimizing carbon oxygen reaction and dephosphorization [1–4]. However, unreasonable blowing will cause slag overflow or metal droplet splash, which not only increases the steel consumption in converter production and pollutes the environment, but also causes major safety accidents. Therefore, the structure of oxygen lance must be designed reasonably in order to realize the safe and efficient operation of converter [5,6]. In recent decades, with the increase of steel production demand and the development of large converters, the oxygen lance has developed from single nozzle structure to porous structure with each nozzle at a certain angle to the axis of the oxygen lance [7–9]. Predecessors have done a lot of research on jet characteristics of oxygen lance and obtained many useful conclusions, which have made an significant contribution to the process optimization and technological innovation of the nozzle [10-15]. However, it is difficult for traditional oxygen lance to meet the needs of high-efficiency and low-cost in the steelmaking process due to the limitation of structural parameters, especially in improving dephosphorization rate [16,17].

Swirl-type oxygen lance is a new type of oxygen lance developed on the basis of traditional oxygen lance (non-swirling oxygen lance), which has developed rapidly in recent years. The main difference between swirl-type oxygen lance and traditional oxygen lance is that the nozzle hole is rotated at a certain angle on the basis of keeping the inclination angle constant. As shown in Figure 1, the inclination angle α is defined as the offset angle of nozzle from vertical direction; the swirl angle β is defined as the included angle of the axis of nozzle of the swirl-type oxygen lance with that of the corresponding traditional nozzle. In the design of oxygen lance, the behavior of oxygen jet can be controlled by adjusting the inclination angle and swirl angle, which improves the operability of oxygen lance. Higuchi et al. studied the behavior of jet and splash of six-hole swirl oxygen lance through water model experiment, and found that the swirl angle of 11.4° was most effective for reducing spillage [18]. Lv studied the stirring effect of swirl-type oxygen lance with different angles on the molten pool. The results showed that the mixing time effect of the 10° swirl-type oxygen lance was

* e-mail: hanpeng@ustl.edu.cn

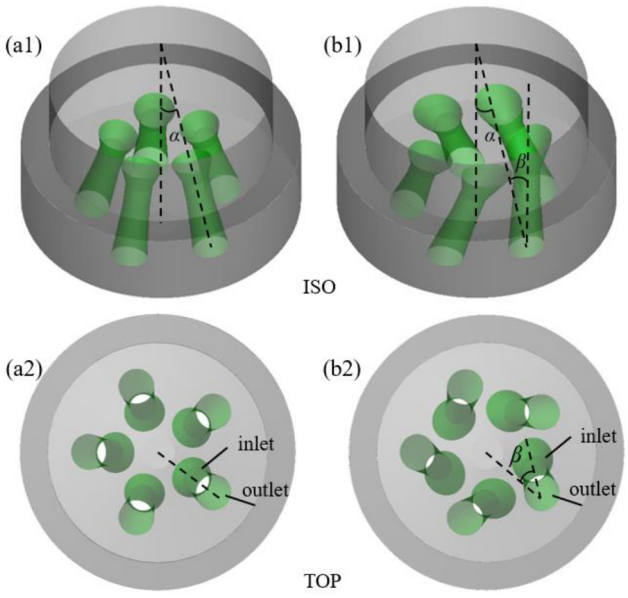

Fig. 1. Schematic diagram of traditional oxygen lance (a) and swirl-type oxygen lance (b).

shortest [19]. Liu considered that the oxygen lance with swirl angle of 8° had the best dephosphorization effect in the 120 t converter through numerical simulation and industrial application [20]. Li also found that the swirl oxygen lance had the advantages of less splashing and strong stirring capacity in the steelmaking process, and believed that the swirl-type oxygen lance had the best stirring effect on the molten pool when the swirl angle was 20° [21]. Li et al. compared the impact area and determined that the best swirl angle was 5° [22].

The above researches enriched the development of swirl-type oxygen lance, but also has limitation, which is that the size of converter is medium in these studies. Nevertheless, the size of converter is 260t in this work. The difference of cubage of converter limits swirl-type oxygen lance industrial application in large-scale converter. In particular, the characteristics of jet under the coupling of inclination angle and swirl angle still need to be further studied.

2 Computational mode

2.1 Model assumptions

This study proposes the following assumptions:
- Gas is Newtonian fluid and compressible.
- The flow of fluid is three-dimensional, steady and non-isothermal.
- The smooth wall surface in the nozzle hole should be avoided and the friction resistance should be ignored.

2.2 Governing equation

The equations involved in this mathematical model include:

Continuity equation:

$$\partial\frac{(\rho u_i)}{\partial x_i}=0 \tag{1}$$

Momentum equation:

$$\partial\frac{(\rho u_i u_j)}{\partial x_j}=-\frac{\partial p}{\partial x_i}+\frac{\partial\left(\tau_{ij}-\rho\,\overline{u_i u_j}\right)}{\partial x_j} \tag{2}$$

Energy equation:

$$\partial\frac{\left[u_i\left(\rho C_p T+p\right)\right]}{\partial x_i}=-\frac{\partial}{\partial x_i}\left(\lambda\frac{\partial T}{\partial x_i}+\frac{C_p\mu_t}{pr_t}\frac{\partial T}{\partial x_i}\right)+\frac{\partial}{\partial x_i}\left(\tau_{ij}u_j-u_j\rho\,\overline{u_i u_j}\right) \tag{3}$$

where ρ is the gas density (kg/m^3); u_i and u_j are the velocity components in the direction of i and j Respectively (m/s); P is the pressure (Pa); C_P is the specific heat capacity, J/(kg·K); λ is the thermal conductivity, W/(m·K); T is temperature (K); Pr_t is the turbulence Prandtl number, $Pr_t=(C_p{\cdot}\mu_t)/\lambda_t$, Pr_t is set as 0.85; τ_{ij} is the viscous stress results due to molecular viscosity (Pa), as defined in equation (4).

$$\tau_{ij}=\mu\left(\frac{\partial u_j}{\partial x_i}+\frac{\partial u_i}{\partial x_j}-\frac{2\partial u_k}{3\partial x_k}\delta_{ij}\right) \tag{4}$$

where δ_{ij} is the Kronecker delta, if $i=j$ or $i\neq j$ therefore $\delta_{ij}=1$ or $\delta_{ij}=0$; μ is the molecular viscosity (Pa·s). The values of the parameters μ were defined in accordance with Sutherland's viscosity in equation (5):

$$\frac{\mu}{\mu_{ref}}=\left(\frac{T}{T_{ref}}\right)^{3/2}\frac{T_{ref}+B}{T+B} \tag{5}$$

where T_{ref} and μ_{ref} are reference temperature and reference viscosity, and B is constant.

The Reynolds stress $-\rho\overline{u_i u_j}$ in the momentum equation is expressed as equation (6) according to Boussinesq hypothesis:

$$-\rho\,\overline{u_i u_j}=\mu_t\left(\frac{\partial u_j}{\partial x_i}+\frac{\partial u_i}{\partial x_j}\right)-\frac{2}{3}\left(\rho k+\mu_t\frac{\partial u_k}{\partial x_k}\right)\delta_{ij} \tag{6}$$

where μ_t is the turbulence viscosity, Pa·s; and k is the turbulence kinetic energy, m^2/s^2.

For the turbulence equations, the previous studies indicate k-ω turbulence model can more accurately describe the behaviors of multi-nozzle jets [22,23]. Compared to the experimental results, the tendency of velocity variation of simulation results fits the physical tendency. The equations of the model are as follows:

$$\frac{\partial(\rho k u_i)}{\partial x_i}=\frac{\partial}{\partial x_i}\left[\left(\mu+\frac{\mu_t}{\sigma_k}\right)\frac{\partial k}{\partial x_j}\right]+G_k-Y_k+S_k \tag{7}$$

$$\frac{\partial(\rho\omega u_i)}{\partial x_i}=\frac{\partial}{\partial x_i}\left[\left(\mu+\frac{\mu_t}{\sigma_\omega}\right)\frac{\partial\omega}{\partial x_j}\right]-\frac{\alpha\omega^2}{k}G_k-Y_\omega+S_\omega \tag{8}$$

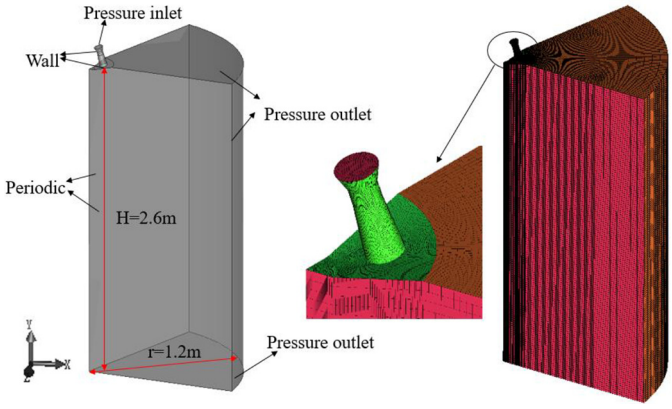

Fig. 2. Computational domain and mesh generation.

The parameter G_k is the generation of turbulence kinetic energy due to mean velocity gradients, and G_ω is the generation of the specific dissipation rate. Y_k and Y_ω are the dissipations of k and ω respectively. S_k and S_ω are the user-defined source terms, and the turbulent viscosity μ_t is modelled by:

$$\mu_t = \frac{\rho k}{\omega} \tag{9}$$

2.3 Calculation domain and solution method

A commercial 260t top blown converter is considered as the object. To improve computational efficiency while ensuring computational accuracy, the model is simplified and 1/5 of the whole calculation domain is simulated. Hexahedron cells are utilized to partition the calculation region to generate grids. Because the velocity gradient in the nozzle outlet area changes greatly, the mesh is encrypted. The computing domain and grid are shown in Figure 2.

The inlet boundary condition is set as the pressure inlet, the outlet boundary condition is set as the pressure outlet and the inner interface is set as the periodic boundary condition. The part of the rest is set as the wall. The near-wall surfaces are treated with standard wall functions, and all normal gradients are zero. Nozzle size and boundary condition values are shown in Table 1. The coupling between pressure and velocity is solved by SIMPLE algorithm. The continuity equation, continuity equation and energy equation are discretized by second-order upwind scheme. The solution is considered to have converged when the numerical residual is smaller than 10^{-6} for energy and less than 10^{-5} for other dependent variables.

2.4 Grid-Independence test

In order to ensure the accuracy and efficiency of the calculation results, four grid schemes A (340868 cells), B (724136 cells), C (1206672 cells) and D (17228882 cells) are selected for calculation. Figure 3 shows the jet velocity distribution of the four grid schemes. H and de are respectively defined as oxygen lance height and outlet diameter of nozzle. H/de is a dimensionless quantity, which represents the distance between oxygen lance and molten pool. It is found that when $H = 20de$, the differences of velocity between gird scheme A, B, C and D are 19.4%, 12.7% and 1.8%, which indicate the velocity distribution of gird scheme C and D is almost the same. In order to economize computing resources, the grid scheme C is used for the subsequent calculations and analysis.

3 Results and discussion

3.1 Validation of simulation

It is essential to verify the accuracy of the mathematical model before its application for numerical simulation. Therefore, the nozzle for 260t converter were machined by reducing three times in proportion and the jet characteristics were tested. The cold test system is shown in Figure 4. An air compressor of 75 Kw and a surge tank with an effective volume of 3 m^3 was used to establish a stable pressure of 10 Kpa. A control station with 64 speed sensors was positioned in front of the nozzle. A computer was applied to store data. Figure 5 shows the comparison of the simulated velocity of jet at different axial distances with the experimental data. The showed that the simulation results are in good agreement with the experimental results.

3.2 Jet characteristics

3.2.1 Velocity distribution

In the steelmaking process, the impact strength of jet on the molten pool determines the cavity depth. Therefore, the decay of jet velocity has an important influence on the stirring effect of the molten pool. Figure 6 displays the distribution of jet velocity with different inclination and swirl angles at different axial distances. It can be found that at the same axial distance, the jet velocity of swirl-type oxygen lance is lower than that of traditional oxygen lance ($\beta = 0°$), and the jet velocity decreases with the increase of swirl angle and inclination angle. In addition, it is found that when the inclination angle or swirl angle is smaller, the interaction between them is more obvious. When $H = 20de$ and $H = 40de$, the jet velocity of swirl-type oxygen lance is less than that of traditional oxygen lance by (28–36) m/s and (17–22) m/s respectively. The differences show that the impact strength of traditional oxygen lance on molten pool is higher than that of swirl-type oxygen lance, but the gap between them gradually decreases with the increase of axial distance.

As is known, the impact force of oxygen jet is the main driving force to promote the stirring of molten pool and the splashing of metal-slag droplets. The jet velocity of swirl-type oxygen lance can be divided into axial velocity, radial velocity and tangential velocity due to unique nozzle structure. Axial velocity determines the cavity depth of the molten pool. Radial velocity affects the distance between jets, which determines the cavity width. Tangential velocity makes the molten steel rotate horizontally, which increases the flow of molten pool and strengthens the reaction between slag and metal [24]. Figure 7 shows the distribution of radial and tangential velocity at $H = 30de$ with different inclination and swirl angles. It is found that

Table 1. Geometric parameters and boundary conditions.

Geometric parameter	Flow rate, Q /Nm^3·h^{-1}	45000, 48000, 51000, 54000. 57000
	Throat diameter, dt /mm	42.6, 44.4, 45.7, 47.1, 48.3
	Outlet diameter, de /mm	57.4, 59.3, 61.1, 63, 64.7
	Number of nozzles, N, –	5
	Inclination angle, α /°	13, 14, 15
	Swirl angle, β /°	0, 5, 8, 10, 12, 15
	Mach number, Ma, –	2.07
Boundary condition	Inlet pressure, P_0/MPa	0.9
	Inlet temperature, T_0/K	300
	Ambient temperature, T_b/K	300
	Ambient pressure, P_b/MPa	0.104

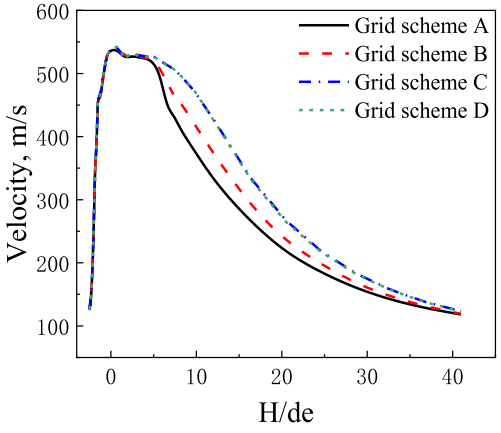

Fig. 3. Distribution of jet velocity with different grid schemes.

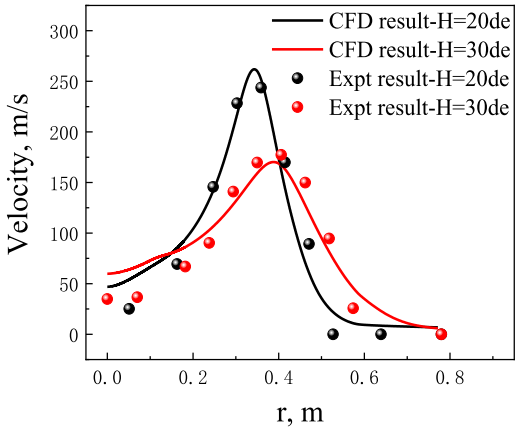

Fig. 5. Radial velocity distribution of the jet at different axial distances.

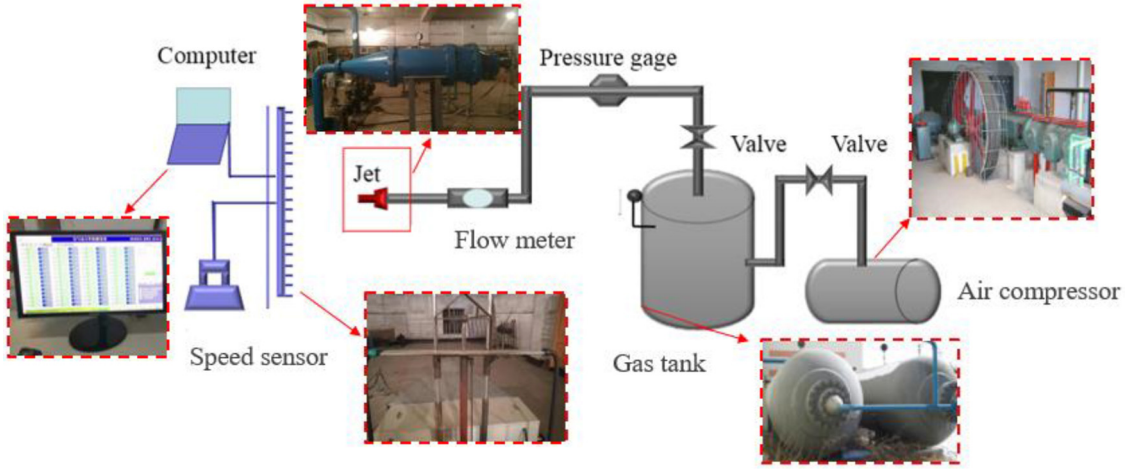

Fig. 4. Schematic of experimental setup.

with the increase of inclination or swirl angle, the radial velocity of the jet increases and the outward expansion aggravates, which is of great significance to increase the contact area between oxygen and metal. However, it may also lead to the converter lining eroded by the oxygen jet. Different from the radial velocity, the tangential velocity increases with the increase of swirl angle, but decreases with the increase of inclination angle. As can be seen from Figure 7b, it is more effective to increase the tangential velocity by increasing the swirl angle at lower inclination angle. Furthermore, the stirring intensity of swirl jet to molten pool depends on the cooperative action of inclination angle and swirl angle on the premise of determining other operating conditions.

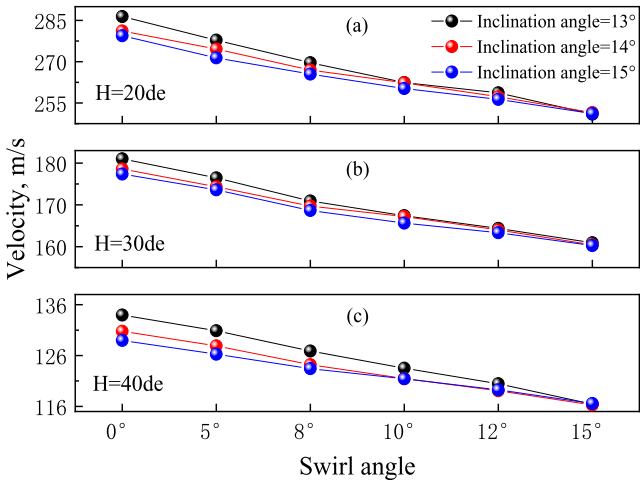

Fig. 6. Distribution of Jet velocity at different axial distances.

3.2.2 Temperature distribution

Figure 8 displays the temperature distribution of jet during movement at different swirl and inclination angles. It can be seen from figure that temperature of the jet gradually increases after it leaves the nozzle exit. The reason is that the jet exchanges heat with the environment due to turbulent entrainment, so that the temperature of jet gradually tends to the ambient temperature. The temperature of swirling jet is higher than that of traditional jet, which increases with the increase of swirl angle at the same axial distance. It indicates that compared with the traditional jet, each jet of the swirl-type oxygen lance is more independent and can fully exchange heat with the environment. The influence of inclination angle on temperature distribution is similar to that of swirl angle, and the jet temperature increases with the increase of inclination angle.

3.2.3 Axis of oxygen lance

The distribution of velocity along the axis of the oxygen lance reflects the interaction between the multi-nozzle oxygen lance jets, which is closely related to the structure of the oxygen lance [23]. Figure 9 shows the distribution of velocity along the axis of oxygen lance with inclination angle and swirl angle. It can be found that the velocity on the axis of oxygen lance is close to 0 when $H = (0–7)de$. With the increase of axial distance, the jet velocity gradually increases. It can be predicted that with the further increase of axial distance, the jet velocity on the central axis of the oxygen lance will reach a maximum, and then gradually decrease, which indicates that the jet entrains the environment gas and interferes with each other in the process of movement. The velocity along the axis of the oxygen lance gradually increases due to the influence of jet motion. In addition, it is also found that the velocity along the axis of oxygen lance decreases with the increase of swirl angle or inclination angle, which indicates that larger swirl angle or inclination angle can reduce the interference between jets and improve independence between jets.

Due to the intense reaction between slag and metal in the blowing process, high-temperature slag may adhere to the surface of nozzle, which not only reduces the cooling effect of nozzle, but also erodes metal materials of the nozzle surface. Moreover, the phenomenon may cause the deformation of the nozzle hole and deteriorate the characteristics of jet. Therefore, it is essential to pay attention to the distribution of pressure within range of nozzle outlet [12]. Figure 10 indicates the distribution of static pressure along the axis of the oxygen lance with inclination angle and swirl angle. It is found that the static pressure near the nozzle outlet is lower than the ambient pressure and gradually approaches the ambient pressure with the increase of axial distance. It can be seen that the static pressure gradually decreases with the increase of swirl angle or the decrease of inclination angle at the same axial distance, but the static pressures change very little with inclination angle when $H > 20de$, which indicates that the larger swirl angle or the smaller inclination angle may cause slag sticks to the nozzle surface and reduce the life of nozzle.

3.3 Jet coalescence

A study on coalescence of jets from traditional oxygen lance under different key variables and operational conditions confirmed that the coalescence pattern was favorable in predicting the dynamics of the jets and estimating the interactions of the jets with bath while splashing characteristics in BOF [17]. Generally, more intensive coalescence can delay the attenuation of jet, which maintains greater penetrating and stirring abilities to the bath. However, coalescence of the jets reduces the impact area on the molten pool. Therefore, the inclination and rotation angle of the nozzle need to be strictly designed to obtain the ideal impact area.

Figures 11 and 12 show the jet coalescence with different inclination angles and swirl angles. It can be seen that each individual jet gradually deviates from the nozzle axis due to the effect of inclination angle, and then is clustered in the nozzle axis and eventually tends to unify in the movement process of jet. This phenomenon is caused by the interaction of multiple jets in the process of flow diffusion. Under the effect of swirl angle, the jet morphology changes and the outward expansion of jets intensifies, which weakens the effect between jets. The larger swirl angle makes the phenomenon clearer. In contrast, the inclination angle only affects the distance between jets, which means that the swirl-type oxygen lance can effectively reduce the jet coalescence and slag splashing at the same inclination angle compared to traditional oxygen lance. Therefore, the inclination angle of swirl-type oxygen lance can be reduced accordingly in order to maintain the impact strength to molten pool while the swirl angle is increased.

To quantitatively analyze the coalescence extent of the swirl jet, the shift distances are defined as the deviation of jet center from the lance axis. Figure 13 shows the shift distances at different axial distances and various inclination and swirl angles. The results demonstrate that at different axial

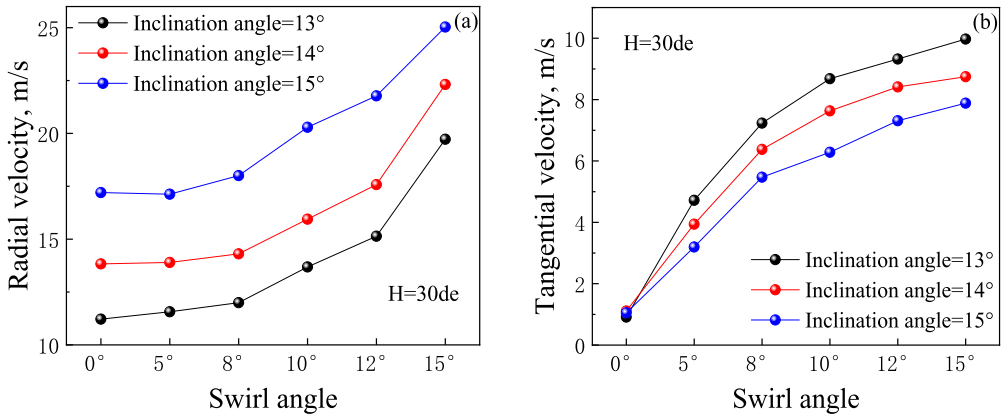

Fig. 7. Distribution of radial and tangential velocity with angle at different axial distance.

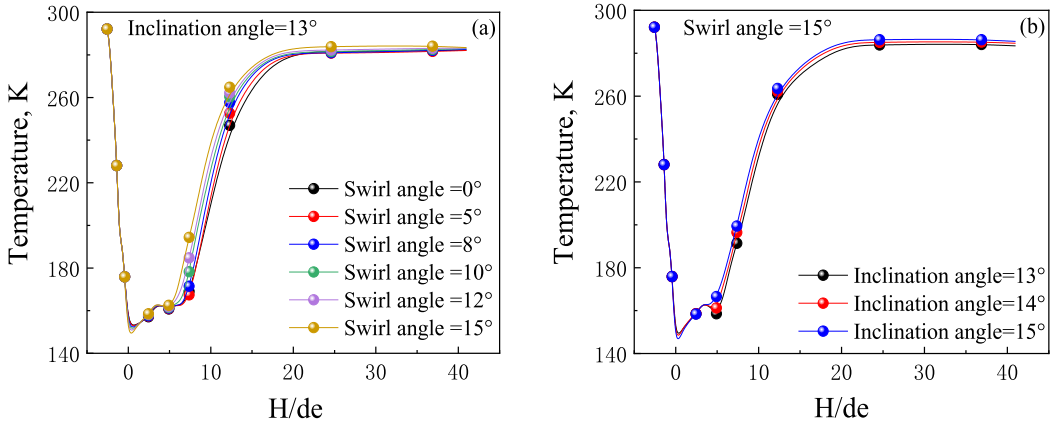

Fig. 8. Distribution of temperature with angle at different axial distance.

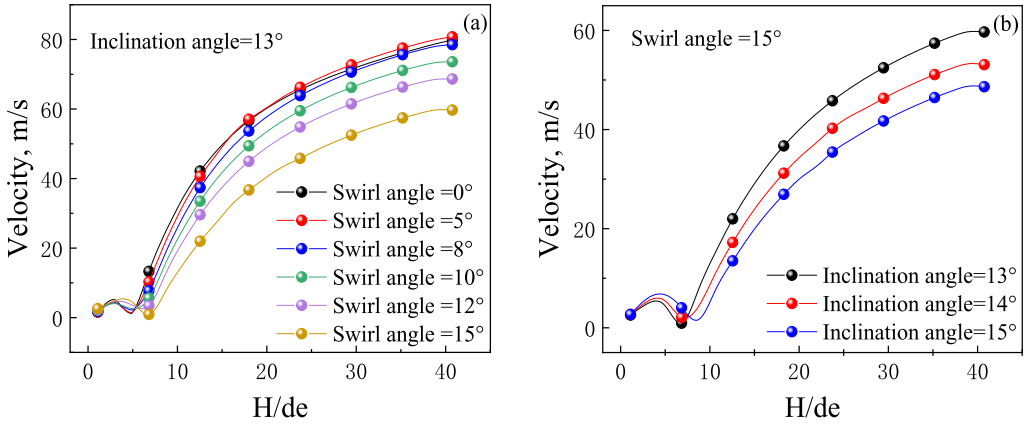

Fig. 9. Distribution of velocity along axis of oxygen lance with angle at different axial distance.

distances, the shift distance increases by 9.65% for every 1° increase in inclination angle; for every 5° increase in swirl angle, the shift distance increases by 9.46%. Furthermore, it can be clearly seen that when $H = 40de$, the change of shift distance is most obvious by changing the swirl angle or inclination angle. In practical application, greater shift distance implies a more dispersive position where the jets impinge directly onto the bath surface. As a result, the subsequent unit phenomena can be improved by obtaining well-proportioned stirring of the bath and promoting flow to be homogeneous in the converter [24].

In order to further quantitatively clarify the swirl-type oxygen lance, a deviation angle (referring to Φ) is defined as the rotational angle of a swirling individual jet center departing from that of traditional oxygen lance at horizontal plane [22]. The larger deviation angle represents

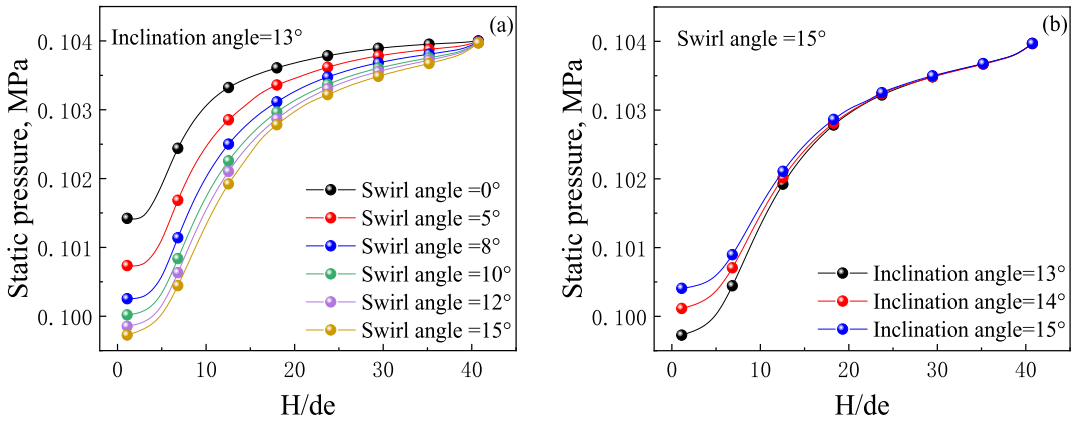

Fig. 10. Distribution of static pressure along axis of oxygen lance with angle at different axial distance.

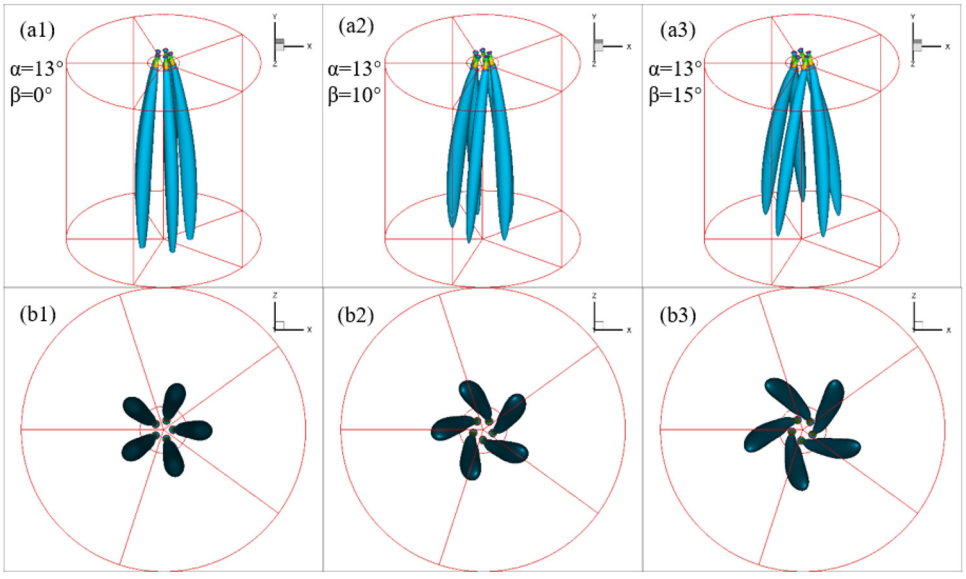

Fig. 11. Variation characteristics of jet coalescence with swirl angle.

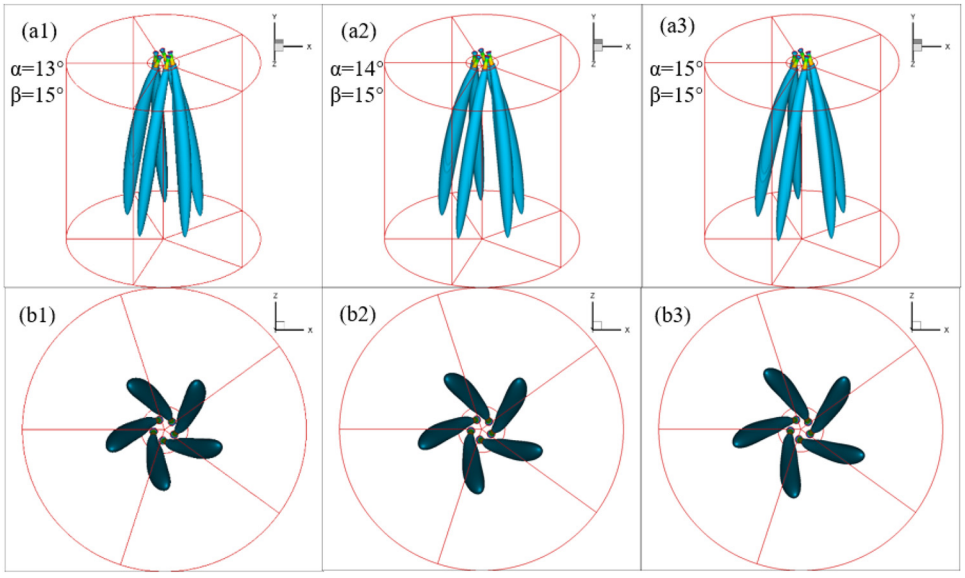

Fig. 12. Variation of jet coalescence with inclination angle.

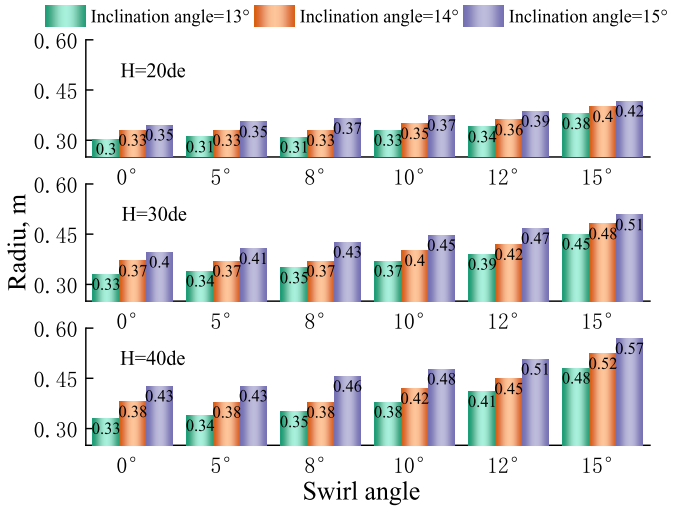

Fig. 13. Variation of shift distance with inclination angle and swirl angle.

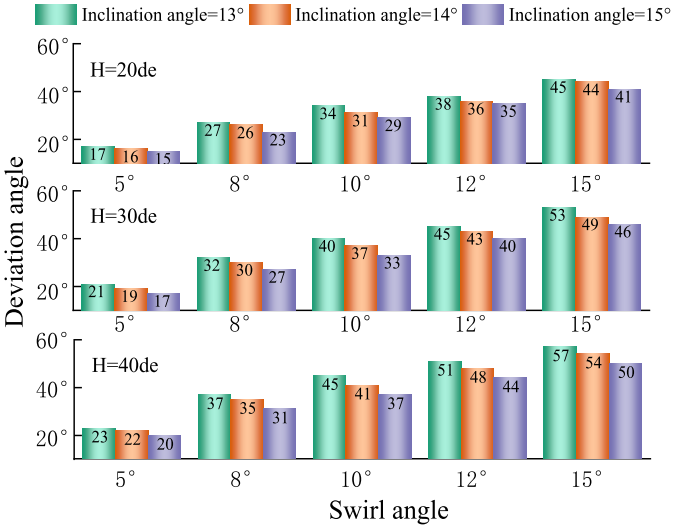

Fig. 14. Variation of deviation angle with inclination angle and swirl angle.

the greater intensity of swirling jet flow. Apparently, Φ is 0 for the traditional jet. Figure 14 shows the effect of the inclination angle and swirl angle on the deviation angle at different axial distances. It can be seen that the deviation angle tends to be larger with the increase of swirl angle or the axial distance. However, the deviation angle decreases with the increase of inclination angle when other variables keep constant. This is consistent with the variation of tangential velocity with inclination angle and swirl angle, which indicates that tangential velocity determines the swirl intensity of swirl-type oxygen lance. In this research, the maximum deviation angle can be obtained when the inclination angle is 13° and the swirl angle is 15°. These results indicate that the flow of the swirling jet can be intensified by increasing the swirl angle or decreasing the inclination angle.

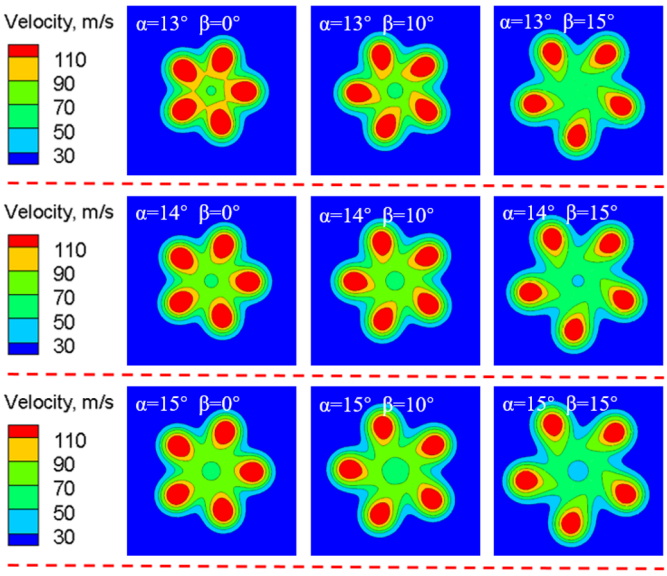

Fig. 15. Jet velocity distribution with different swirl angles and inclination angles at $H = 30de$.

3.4 Jets cross-sectional area

In BOF practices, the impact area of the jets was applied to evaluate the cavity width, and the axial velocity magnitude determines the cavity depth [25]. The depth and width together determine the shape and size of the cavity. The deeper cavity depth accelerates the flow velocity of liquid steel on the surface of the bath, while the wider cavity diameter enhances the uniform distribution of radial velocity in the molten steel and increases the flow velocity of molten steel at the bottom of furnace hearth [2].

Figure 15 shows the jet velocity distribution of oxygen lance with different swirl angles and inclination angles at $H = 30de$. The results show that increasing the inclination angle enhances the outward movement of jet, making each jet tend to separate and resulting in the expansion of the jet boundary to the surrounding environment, which will not only increase the contact area between the jet and the molten pool, but also reduce the possibility of jet coalescence. However, it may weaken the mixing effect of the jet to the molten pool and aggravate the scour of the jet to the converter lining. In addition, the swirl angle also makes the jet rotate counterclockwise in the horizontal direction, which strengthens the stirring of the molten pool.

To quantify the radial spreading of the jets in the process of movement, the impact area of jet surrounded by different isokinetic lines with different swirl angles and isokinetic lines is measured by *Image J* software, as shown in Figure 16. The results demonstrate that when the isokinetic line is >90 m/s, the impact area decreases with the increase of swirl angle; When the isokinetic line = 70 m/s and the swirl angle is 10°, the impact area reaches the peak; When the isokinetic line is >50 m/s, the impact area increases with the increase of swirl angle.

Cai considered that the corresponding velocity of oxygen jet to break through the slag layer and contact with molten iron is the effective velocity, and the effective

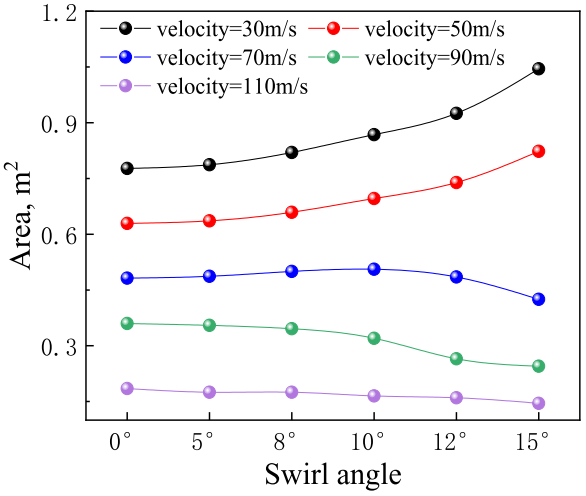

Fig. 16. Impact area distribution with different swirl angles and isokinetic lines at $H = 30de$.

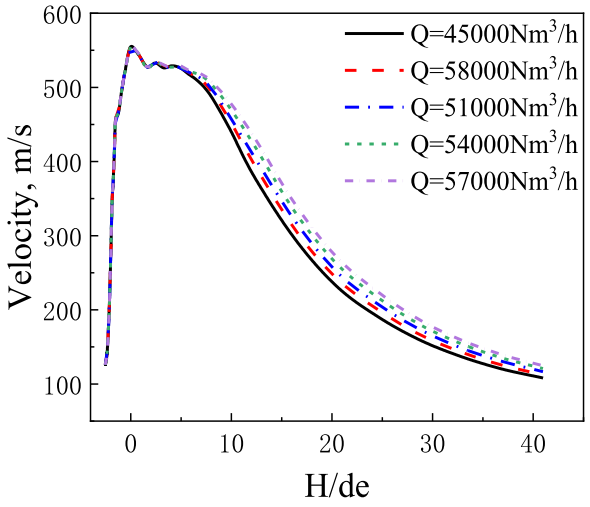

Fig. 18. Distribution of jet velocity with different flow rates.

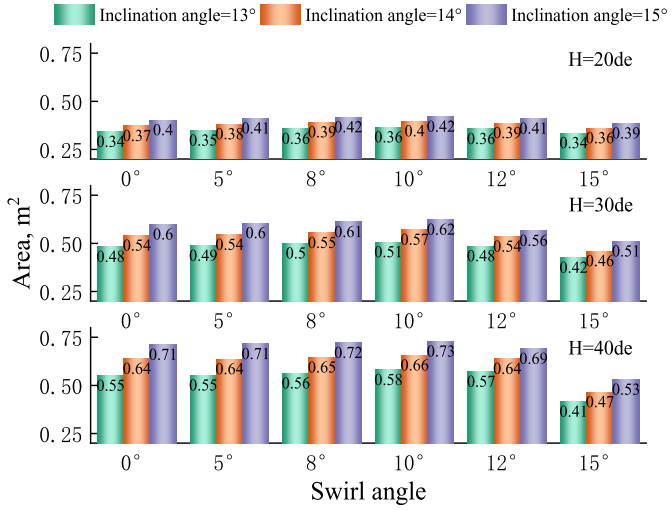

Fig. 17. Effective impact area distribution with different swirl angles and inclination angles.

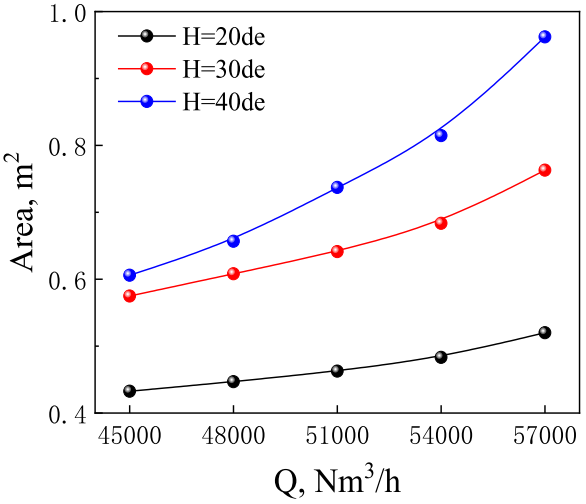

Fig. 19. Effective impact area distribution with different flow rates.

velocity had been calculated was about 74 m/s [26]. Therefore, this study defines the effective impact area of the jet on the molten pool as the area surrounded by the isokinetic line 70 m/s, and further analysis is carried out. Figure 17 shows that in the ranges of current condition, the effective impact area of jet increases with increasing axial distance and inclination angle, whereas it varies non-monotonously with the swirl angle. Specially, the impact area with swirl angle of 10° is found to be the largest. Therefore, the optimum inclination and swirl angle of the swirl-type oxygen lance for a 260t converter are 15° and 10° respectively.

3.5 Variation of flow rate

In order to raise steel production, it is generally to enhance the flow rate to improve the oxygen blowing intensity. However, the changes of flow rate not only influence the decay of jet velocity and operation of oxygen lance, but also affect the effective impact area of jet. Therefore, this manuscript takes the optimized swirl-type oxygen lance with a flow rate of 51,000 m^3/h as object, and designs another four schemes to understand the jet characteristics under different flow rates.

Figure 18 shows the velocity distribution of jet under different flow rates. The result demonstrates that the jet velocity gradually increases with the increase of flow rate, which means that higher flow rate makes the cavity deeper. In order to reasonably evaluate the influence of flow rate on jet mixing efficiency, the effective impact area of jet with flow rate under different axial distances is discussed. As shown in Figure 19, the variation trend of effective impact area of jet with flow rate is consistent under different axial distances, which is area increases with the increase of flow. Moreover, the tendency is more obvious when farther axial distance.

4 Conclusion

The jet characteristics of swirl-type oxygen lance are studied by numerical simulation, and the coupling effect of inclination and swirl angle on jet velocity distribution, jet coalescence and jet impact area are clarified. The results are summarized as follows:

- Compared with the traditional oxygen lance, the swirl-type oxygen lance accelerates the velocity attenuation of the jet. However, the tangential velocity of jet improvers the stirring efficiency of the molten pool, which is conducive to the rapid melting of the slag in the steelmaking.
- With the increase of swirl angle and inclination angle, the velocity of jet decreases, the temperature of jet increases and the independence between jets is improved.
- With the increase of the swirl angle, the tangential velocity of the swirl-type oxygen lance increases, which strengthens the flow of the swirl jet, but the possibility of slag adhering to the nozzle surface increases.
- The effective impact area increases with the increase of inclination angle, but varies non-monotonously with the swirl angle. The optimum inclination and swirl angle of the swirl-type oxygen lance for a 260t converter are 15° and 10° respectively.
- When the oxygen flow rate increases, the decay of jet velocity decreases and the effective impact area increases.

Acknowledgments. The authors are grateful for the financial support by National Key R&D Project of China (2021YFB3702000), The National Natural Science Foundation of China (NSFC) (U20A20272), Key project of Handan Scientific Research Program (21122015004), and State Key Laboratory of Marine Equipment and Applications - University of science technology of Liaoning united fund (HGSKL-USTLN202101).

References

1. N. Asahara, K. Naito, I. Kitagawa, Fundamental study on interaction between top blown jet and liquid bath, Steel Res. Int. **82**, 587 (2011)
2. M. Lv, R. Zhu, Y.G. Guo , Simulation of flow fluid in the BOF steelmaking process, Metall. Trans. B. **44**, 1560 (2013)
3. A. Morshed, N. Jamal, B. Geoffrey, A computational fluid dynamics model of shrouded supersonic jet impingement on a water surface, ISIJ Int. **52**, 1026 (2012)
4. Q. Li, M. Li, S.B. Kuang, Numerical simulation of the interaction between supersonic oxygen jets and molten slag–metal bath in steelmaking BOF process, Metall. Trans. B. **46**, 1494 (2015)
5. R. Sambasivam, S.N. Lenka, F. Durst, A new lance design for BOF steelmaking, Metall. Trans. B. **38**, 45 (2007)
6. J.P. Rao, G.Q. Li, Z.Z. Yang, Research and application of new oxygen lance for BOF steelmaking, Adv. Mater. Res. **74**, 335 (2011)
7. G. Liu, K. Liu, P. Han, Numerical investigation on behaviors of interlaced jets and their interaction with bath in BOF steelmaking, AIP Adv. **9**, 075202 (2019)
8. Y. Tago, Y. Higuchi, Fluid flow analysis of jets from nozzles in top blown process, ISIJ Int. **43**, 209 (2003)
9. I. Sumi, Y. Kishimoto, Y. Kikuchi, Effect of high-temperature field on supersonic oxygen jet behavior, ISIJ Int. **46**, 1312 (2006)
10. R. Sambasivam, F. Durst, Characteristics of supersonic jets in LD steelmaking, Ironmak Steelmak. **37**, 195 (2010)
11. M. Alam, J. Alam, G. Brooks, Computational fluid dynamics simulation of supersonic oxygen jet behavior at steelmaking temperature, Metall. Trans. B. **41**, 636 (2010)
12. M. Li, Q. Li, S.B. Kuang, Coalescence characteristics of supersonic jets from multi-nozzle oxygen lance in steelmaking BOF, Steel Res. Int. **86**, 1517 (2015)
13. M. Li, Q. Li, L. Li, Effect of operation parameters on supersonic jet behavior of BOF six-nozzle oxygen lance, Ironmak Steelmak. **41**, 699 (2014)
14. K. Naito, Y. Ogawa, T. Inomoto, Characteristics of jets from top-blown lance in converter, ISIJ Int. **40**, 23 (2000)
15. Q. Li, M. Li, S. B. Kuang, Computational study on the behaviors of supersonic jets and their impingement onto molten liquid free surface in BOF steelmaking, Can. Metall. Q. **53**, 340 (2014)
16. Z.F. Yuan, Y. Xiao, Z.X. Lu, Jet behavior and metallurgical performance of innovated double-parameter oxygen lance in BOF, J Iron Steel Res. Int. **14**, 1 (2007)
17. G. Liu, K. Liu, P. Han, Metallurgical performance of innovative double-parameter oxygen lance in BOF steelmaking, Ironmak Steelmak. **48**, 437 (2021)
18. Y. Higuchi, Y. Tago, Effect of nozzle twisted lance on jet behavior and spitting rate in top blown process, ISIJ Int. **43**, 1410 (2003)
19. M. Lv, R. Zhu, H. Wang, Simulation and application of swirl-type oxygen lance in vanadium extraction converter, Steel Res. Int. **84**, 304 (2013)
20. F. Liu, D. Sun, R. Zhu, Effect of nozzle twisted oxygen lance on flow field and dephosphorisation rate in converter steelmaking process, Ironmak Steelmak. **44**, 640 (2016)
21. L. Li, M. Li, L. Shao, Physical and mathematical modeling of swirling gas jets impinging onto a liquid bath using a novel nozzles-twisted lance, Steel Res. Int. **91**, 1900684 (2020)
22. M. Li, Q. Li, Z. Zou, Computational investigation of swirling supersonic jets generated through a nozzle-twisted lance, Metall. Trans. B. **48**, 713 (2017)
23. W. Wang, Z. Yuan, H. Matsuura, Three-dimensional compressible flow simulation of top-blown multiple jets in converter, ISIJ Int. **50**, 491 (2010)
24. M. Li, L. Shao, Q. Li, A numerical study on blowing characteristics of a dynamic free oxygen lance converter for hot metal dephosphorization technology using a coupled VOF-SMM method, Metall. Trans. B. **52**, 2026 (2021)
25. L. Yang, Z. Yang, G. Wei, Influence of ambient and oxygen temperatures on fluid flow characteristics considering swirl-type supersonic oxygen jets, ISIJ Int. **59**, 2272 (2019)
26. Z. Cai, Y. Xie, A. Xia, The interaction of supersonic jet on liquid bath in oxygen steelmaking, Iron and Steel. **15**, 14 (1980)

Cite this article as: Xi Wang, Peng Han, Kun Liu, Effect of multi-angle parameter on fluid flow characteristics of swirl-type oxygen lance, Metall. Res. Technol. **119**, 314 (2022)